Pyroelectric and photovoltaic properties of Nb-doped PZT thin films

A. Berenov, P. Petrov, B. Moffat, J. Phair, L. Allers, and R. W. Whatmore

COLLECTIONS

Paper published as part of the special topic on 100 Years of Ferroelectricity - a Celebration

View Online   Export Citation   CrossMark

ARTICLES YOU MAY BE INTERESTED IN

Epitaxial ferroelectric oxides on silicon with perspectives for future device applications
APL Materials 9, 040701 (2021); https://doi.org/10.1063/5.0039161

Low temperature growth of epitaxial ferroelectric BaTiO$_3$
APL Materials 9, 041104 (2021); https://doi.org/10.1063/5.0046624

Cantilever magnetoelectric PZT/Tb–Fe–Co resonators for magnetic sensing applications
APL Materials 9, 041103 (2021); https://doi.org/10.1063/5.0042379

Pyroelectric and photovoltaic properties of Nb-doped PZT thin films

View Online   Export Citation   CrossMark

A. Berenov,[1,a]   P. Petrov,[1]   B. Moffat,[2]   J. Phair,[2]   L. Allers,[3]   and R. W. Whatmore[1]

AFFILIATIONS

[1] Department of Materials, Imperial College London, London SW7 2AZ, United Kingdom
[2] Pyreos Ltd., Heriot Watt Research Park, Edinburgh EH14 4AP, United Kingdom
[3] Korvus Technology Ltd., Tavistock PL19 8AB, United Kingdom

Note: This paper is part of the Special Topic on 100 Years of Ferroelectricity—A Celebration.
[a]Author to whom correspondence should be addressed: a.berenov@imperial.ac.uk

ABSTRACT

Nb-doped lead zirconate titanate (PZT) films with up to 12 at. % of Nb were co-sputtered from oxide PZT and metallic Nb targets at a substrate temperature of 600 $^\circ$C. Up to 4 at. % of Nb was doped into the perovskite structure with the formation of B-site cation vacancies for charge compensation. The preferential (111) PZT orientation decreased with Nb-doping within the solid solution region. The ferroelectric response of the films was affected by the large values of the internal field present in the samples (e.g., -84.3 kV cm^{-1} in 12 at. % Nd doped films). As-deposited unpoled films showed large values of the pyroelectric coefficient due to self-poling. The pyroelectric coefficient increased with Nb-doping and showed a complex dependence on the applied bias. The photovoltaic effect was observed in the films. The value of the photocurrent increased with the A/B ratio. The combined photovoltaic–pyroelectric effect increased the values of the measured current by up to 47% upon light illumination.

INTRODUCTION

Lead zirconate titanate (PZT) perovskites with the general formula Pb(Zr$_x$Ti$_{x-1}$)O$_3$, PZTx/(1 − x), are used extensively in a variety of device applications, such as piezoelectrics and pyroelectrics. Enhanced piezoelectric properties are observed in the compositions close to the morphotropic phase boundary (MPB) at x = 0.53, where rhombohedral and tetragonal phases coexist. The properties of the material can further be tailored by the doping on either A or B sites in the perovskite structure.[1,2] Isovalent doping (e.g., Ba^{2+} on the Pb^{2+} site or Sn^{4+} on the Ti^{4+}/Zr^{4+} site) lowers the Curie temperature, T$_C$, and increases the permittivity. Acceptor doping (e.g., K$^+$ on the Pb^{2+} site or Fe^{3+} on the Ti^{4+}/Zr^{4+} site) increases the concentration of oxygen vacancies, which are regarded as efficient pinning sites, and decreases domain wall movement. Consequently, permittivity and dielectric losses decrease and the mechanical quality factor of piezoelectric materials increases. Donor doping (e.g., La^{3+} on the Pb^{2+} site or Ta^{5+} on the Ti^{4+}/Zr^{4+} site) reduces oxygen vacancy concentration and increases domain wall movement. As a result, the permittivity and piezoelectric coefficient increase and leakage current decreases. Donor doping of Nb^{5+} in PZT is usually reported to occur on the B-site and is accompanied by the creation of a positively charged defect, Nb$_{Ti}$. The defect charge compensation is achieved by the reduction in the concentration of oxygen vacancies and/or formation of cation vacancies (e.g., V''_{Pb}). A decrease in the oxygen vacancies on the surface was observed from XPS measurements of PZT52/48 sputtered films[3] and by photoluminescence in 13 at. % Nb-doped sputtered PZT52/48 films.[4] A-site doping of Nb in PZT has also occasionally been proposed.[5–7] Nb-doping in PZT increases the dielectric constant and remanent polarization, reduces the leakage current,[8] and improves the fatigue performance.[4,9] Enhanced performance of Nb-doped PZT devices due to higher values of piezoelectric[10,11] and pyroelectric coefficients[12,13] has been reported.

Nb-doping in bulk PZT has been extensively studied.[14,15] Thin films typically showed better properties as compared with the bulk. In most cases, Nb-doped thin films were prepared by the sol–gel method due to its simplicity.[5,6,9,10,12,13,16–25] However, physical vapor deposition methods offer an alternative that fits better with well-established industrial process lines. Methods include pulsed laser

deposition[13,26] and (predominantly) sputtering.[27] Due to volatility of Pb at sintering or crystallization temperatures, an excess of lead is usually employed during the synthesis. Sputtering from single ceramic targets[3,4,8,27,28] or reactive sputtering from individual metal targets[29,30] has been performed. Compositions of single ceramic targets are selected to be close to the intended compositions of the deposited films, with the exception of the Pb content. 30 at. % Pb excess was used in the targets for 13 at. % Nb-doped PZT52/48 film deposition.[4] No Pb excess was employed in the targets for 14 at. % Nd doped PZT52/48 deposition at 660 °C for 4 h in Ar.[3] Pb deficiency was intentionally introduced in the target compositions during the deposition of PZT54/46 films based on the assumption that $Nb_{Ti}^{\cdot}$ defects are compensated by Pb vacancies.[8,28]

In this work, the effect of Nb-doping in Ti-rich tetragonal PZT30/70 composition was evaluated to assess the potential of such compositions for pyroelectric applications. The films were grown by co-sputtering from ceramic PZT and metallic Nb targets. A detailed evaluation of the ferroelectric and pyroelectric properties is provided as well as photovoltaic response.

EXPERIMENTAL

Nb-doped PZT films were co-sputtered using a "HEX" modular deposition system (Korvus Technology, UK). PZT was sputtered from a 2-in. $Pb_{1.3}Zr_{0.3}Ti_{0.7}O_3$ oxide target at 150 W RF power (13.56 MHz, 17.7 W cm^{-2}) from an R301 power supply (Seren IPS, Inc., USA). The Pb excess was incorporated into the PZT oxide targets to compensate for the Pb losses normally observed with evaporation at high substrate temperatures. Nb was co-sputtered from a 2-in. high purity (>99.9%) Nb metal target at 5–20 mA DC (Table I) current from a GEN600 power supply (TDK Lambda, USA). The substrates were $2 \times 2\,cm^2$ Pt/TiO$_2$/Si wafers. The substrate temperature was calibrated using an Optris PI 1M IR camera (Optris GmbH, Germany), and substrates were allowed to dwell for 30 min prior to film deposition to attain a constant temperature. A substrate temperature of 600 °C was used, as it was shown to be optimum for the formation of single phase PZT films.[16] The deposition was done in an oxidizing gas atmosphere of 80:20 Ar/O$_2$ mixture at 6.1×10^{-3} mbar for 4 h, and samples were allowed to cool in the same gas atmosphere after the deposition. No post-growth anneals were performed.

Film thicknesses were measured with a D-600 profilometer (KLA-Tencor, USA) and were found to be around 620 nm, corresponding to a deposition rate of about 2.6 nm/min. The crystallinity of the films was studied by XRD using an X'Pert diffractometer (Malvern Panalytical, Netherlands) equipped with a 4 axis

goniometer using Cu$_{K\alpha}$ radiation. Film composition was measured with an Epsilon 3 X-ray Fluorescence (XRF) spectrometer (Malvern Panalytical, Netherlands) using the Stratos software module for thin film analysis. Au(40 nm)/Ti(10 nm) top electrodes of 0.5, 1, 2, and 3 mm diameter were sputtered at room temperature from metal sources. Dielectric properties were measured with a 4263B LCR meter (HP, USA), and ferroelectric characterization was performed using a ferroelectric tester with a Trek high voltage amplifier (Radiant Technologies, USA). Small thermal oscillations (±2 K) were generated using a Peltier element, and the resulting pyroelectric current was measured using a 6517B electrometer (Keithley Instruments, USA). At least five thermal cycles were used for the calculation of the pyroelectric coefficient. The frequency of the thermal oscillations (0.05 Hz) was selected in order to achieve uniform heat propagation in the film thickness.[31] Several measurements were performed under light illumination provided by a 150 W halogen spectrally broad lamp probe illumination (ACE Light Source, Schott). The optical power was measured with an optical power meter (PM100A, ThorLabs).

RESULTS AND DISCUSSION

The XRD patterns of the deposited films (Fig. 1) show predominant formation of the tetragonal PZT phase with very strong (111) crystal orientation. Occasionally, the "forbidden" (200) Si reflection was detected due to multiple diffraction.[32] Pyrochlore phase peaks were also present. The fraction of the pyrochlore phase was calculated as $\frac{\sum I(pyrochlore)}{\sum I(pyrochlore)+\sum I(perovskite)}$, where I(pyrochlore) and I(perovskite) are the integrated intensities of pyrochlore and perovskite peaks, respectively, and is shown as a function of Nb-doping in Fig. 2. Nb-doping resulted in a decrease in the pyrochlore fraction to a minimum value (0.5%) at 4 at. % Nb-doping, which is estimated as the Nb solubility limit in these co-sputtered PZT30/70 films. This value for the Nb solubility limit agrees reasonably well with the values reported in the literature. In the bulk, the extent of Nb-doping was 7 at. % in PZT65/35.[14] For sol–gel PZT films with compositions near the MPB, the solubility limits were reported as 3 at. % Nb for PZT53/47 grown at 680 °C,[25] 4 at. % for PZT53/47 grown at 700 °C,[5] and 5 at. % Nb for PZT53/47 grown at 600[22] and 700 °C.[17] Higher solubility limits were observed for sputtered films: 7 at. % Nb for PZT54/46 films grown at 625 °C[28] and 13 at. % Nb for PZT52/48 films grown at 525 °C.[27] In the Ti-rich PZT compositions, sol–gel films with the solubility limits of 4 at. % Nb in PZT40/60 grown at 650 °C[21] and 4 at. % Nb in PZT20/80 grown at 650 °C[12] were prepared. An increased amount of the pyrochlore phase observed in 8 and 12 at. % Nb films was caused by the

TABLE I. Thickness, composition, and dielectric properties of deposited films.

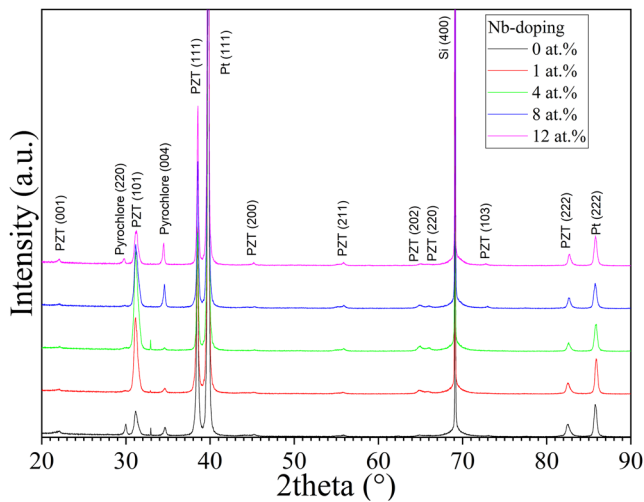| Nb-doping (at. %)	DC current of Nb source (mA)	Film thickness (nm)	Composition	ε_r	tan δ
0	0	623 ± 54	$Pb_{1.01}Zr_{0.31}Ti_{0.69}O_3$	192	0.015
1	5	602 ± 47	$Pb_{1.03}Zr_{0.30}Ti_{0.69}Nb_{0.01}O_3$	181	0.024
4	10	625 ± 17	$Pb_{1.05}Zr_{0.29}Ti_{0.67}Nb_{0.04}O_3$	243	0.019
8	15	622 ± 53	$Pb_{1.03}Zr_{0.28}Ti_{0.65}Nb_{0.08}O_3$	241	0.016
12	20	683 ± 54	$Pb_{1.00}Zr_{0.26}Ti_{0.62}Nb_{0.12}O_3$	280	0.019

FIG. 1. XRD scans of Nb-doped PZT films grown at 600 °C.

stabilization of the pyrochlore phase with Nb-doping in sol–gel films.[17,18]

The degree of preferred (hkl) orientation in the PZT films was calculated as $\frac{I(hkl)}{\sum I(perovskite)}$, where I(hkl) is the integrated intensity of the perovskite PZT (hkl) peak and is shown for (111) and (101) peaks as a function of Nb-doping in Fig. 2. Undoped PZT films show a significant fraction of grains with (111) orientation perpendicular to the film surface. Nb-doping resulted in a decrease in (111) fraction up to 4 at. % Nb-doping followed by an increase. An opposite trend was observed for the (101) fraction, which reached a maximum at 4 at. % Nb-doping. The degree of preferred orientation in the deposited films is influenced by the kinetics of nucleation and grain growth, which are determined themselves by the orientation
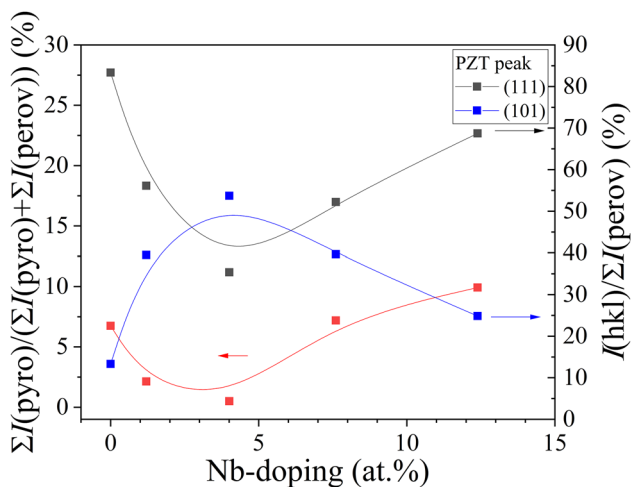
and nature of the substrate, thermodynamics of the film termination surface of the film under the deposition and/or annealing conditions, etc. As a result, PZT film orientations strongly depend on the experimental conditions with the strong effect of the orientation of the substrate. On Pt (111) surfaces, a preferential (111) PZT orientation was reported in Nb-doped sol–gel PZT53/47 films[17,25] and sputtered Nb-doped PZT54/46 films.[28] It was suggested that the (111) orientation has higher crystallization energy and require a seed layer to become preferential during the growth.[12] The nucleation of the (111) PZT orientation is facilitated by the (111) layer of the Pt_3Pb intermetallic compound usually observed during the growth on (111) Pt.[17,33,34] In addition to the strong (111) orientation on (111) Pt peaks, the (100) orientation was also observed in sol–gel PZT53/47[16] and sputtered PZT45/55 films at 600 °C.[35] The predominant (100) orientation of PZT on the Pt (111) substrate can be achieved either by intentional deposition of the PbO seed layer on Pt (111) prior to sol–gel deposition of PZT30/70 films[10] or by assumed pre-deposition of Pb-rich phases (e.g., PbO_2) during sputtering of PZT52/48 films at around 600 °C.[4] Nb-doping has also been reported to affect the preferred orientation in the films. An increase in Nb-doping changed the film orientation from (110) at 0.5 at. % Nb to (100) at 1 at. % Nb in sol–gel PZT40/60 films grown at 700 °C.[23] The maximum degree of the (100) orientation in PZT52/48 films was observed at 4 at. % Nb with the decrease at higher doping levels explained by the accumulation of PbO on the grain boundaries, thus impeding the grain growth of the (100) orientation.[9] At the same time, the change from the (100) orientation on Pt (111) in undoped sol–gel PZT52/48 films to randomly oriented grains upon Nb-doping was observed in PZT52/48 films and was related to the extended (4 h) deposition time.[3]

The lattice parameters as a function of Nb-doping are shown in Fig. 3. The a-lattice parameter decreased up to 4 at. % doping and then increased, whereas the c-lattice parameter exhibited an opposite trend. As a result, the tetragonality, expressed as c/a, reached maximum at 4 at. % Nb-doping. The unit cell volume decreased with Nb-doping (Fig. S1 of the supplementary material). This agrees with
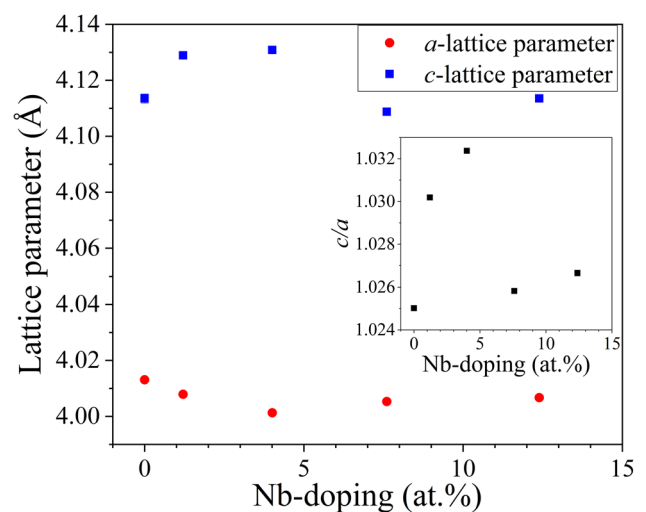

FIG. 2. The effect of Nb-doping in PZT films on the ratio of pyrochlore peak intensities to the combined perovskite and pyrochlore peak intensities (left) and the perovskite (111) and (101) peak intensities to the total perovskite peak intensities (right). Solid lines are guide for the eye.

FIG. 3. Lattice parameters and c/a ratio (inset) as a function of Nb-doping.

previous work, which showed that doping of the smaller Nb^{5+} ion onto the B-site resulted in a decrease in unit cell volume, in general. However, individual reports on lattice parameter dependences with doping showed some complexity. For example, in sol–gel PZT53/47 films grown at 700 °C, the a-lattice parameter increased slightly and the c-lattice parameter significantly decreased with Nb-doping, resulting in the decrease in c/a ratio,[17] whereas in sol–gel PZT53/47 films annealed at 700 °C, the a-lattice parameter decreased up to 8 at. % and then increased with Nb-doping.[5] The attempted Nb-doping on the A-site in PZT53/47 ceramics resulted in non-monotonic changes in lattice parameters with the minimum value of c/a ratio at 4 at. % Nb-doping.[7]

The compositions of the films are shown in Table I assuming that Nb-doping is entirely on the B-site, which is normalized to 1. The Zr/(Zr + Ti) ratio is constant at 0.3 and agrees with the value in the PZT sputter target. The Pb/(Zr + Ti) ratio increased monotonically with Nb-doping from 1.01 in undoped PZT to 1.14 in 12 at. % Nb-doped films. The Pb/(Zr + Ti) ratio observed in the films is lower than the one in the PZT target [Pb/(Zr = Ti) = 1.3], even though the operational parameters of the RF magnetron used for the PZT target were kept constant. Previous work showed that sputtering from a single target with Pb/(Zr + Ti) = 1.3 resulted in the deposition of films with a lower Pb/(Zr + Ti) ratio of 1.1, without observation of any Pb-rich secondary phases.[27] The observed lower Pb content in the films compared with the target compositions is due to the increased volatility of Pb at high temperatures. In addition, self-stabilization of the Pb content during the deposition of $PbTiO_3$ films has been observed, whereby an increase in Pb flux does not lead to an increase in Pb content in the films. This was due to a higher rate of PbO evaporation when the A/B ratio in formed films exceeded 1.[30] The A/B ratio Pb/(Zr + Ti + Nb) observed in our films is close to 1 and showed the maximum value of 1.05 at 4 at. % Nb-doping. A maximum Nb-doping of 12 at. % was achieved (Table I) when a 20 mA current was applied to the Nb metal target.

As the XRD shows that there is practically one single perovskite phase in the 4 at. % Nb-doped film, we need to assign the Pb/(Zr + Ti + Nb) ratio of 1.05 to the perovskite phase. The generally

accepted defect model of Nb-doped PZT includes formation of negatively charged Pb vacancies, V_{Pb}'', to compensate positive defects, $Nb_{Ti}^{•}$, when Nb^{5+} replaces Ti^{4+} on the B-site, resulting in the formula $Pb_{1-\frac{x}{2}}(Zr, Ti)_{1-x}Nb_x O_3$ and Pb/(Zr + Ti + Nb) ratios less than 1.[24,28] The Pb/(Zr + Ti + Nb) ratio in our films is greater than 1, and no formation of Pb-rich secondary phases (e.g., PbO when exceeding solubility limits in PZT53/47[22]) was observed by XRD. Pb/(Zr + Ti + Nb) ratios greater than 1 can be achieved by redistribution of Pb on B-sites as Pb^{4+}. The accommodation of Pb excess by the formation of Pb^{4+} on the B-site was shown in sputtered $PbSc_{0.5}Ta_{0.5}O_3$ films.[36] In sputtered PZT45/55 films with a large A/B ratio of 1.38, the presence of Pb on the B-site was confirmed from the calculated neutron scattering factors assuming that Pb is distributed on both A and B sites.[35] In the PZT52/48 film sputtered at 525 °C in an Ar/O_2 mixture with a Pb/(Zr + Ti + Nb) ratio of 1.1, a charge compensation of $Nb_{Ti}^{•}$ by Pb vacancies is suggested with the redistribution of Pb on the B-site as Pb^{4+}, resulting in the formula $(Pb_{0.94}^{2+}V_{Pb}''')(Pb_{0.076}^{4+}Zr_{0.388}Ti_{0.416}Nb_{0.12})O_3$.[27] However, the introduction of larger Pb^{4+} ions (ionic radii of 0.775 Å[37]) on the B-site with the average ionic radii of 0.64 Å in PZT30/70 is expected to increase the cell volume, as was observed in $PbSc_{0.5}Ta_{0.5}O_3$[36] and PZT45/55,[35] whereas the introduction of Nb^{5+} (0.64 Å) is likely to cause negligible volume changes. No unit cell volume increase was observed in this work; indeed, we see a slight decrease (Fig. S1 of the supplementary material). As a result, we could speculate that $Nb_{Ti}^{•}$ defects are compensated by the formation of vacancies on the B-site, presumably due to the large Pb excess in the PZT target [Pb/(Zr + Ti) = 1.3] used in this work. The presence of B-site vacancies was detected by positron lifetime measurements in PZT40/60[38] and lanthanide-ion-doped $PbTiO_3$[39] ceramics. Furthermore, the association of the point defect into clusters is possible at the doping levels studied in this work. For example, the formation of V_{Pb}–nV_O defect clusters was suggested in 8 at. % Ln (La–Eu) doped $PbTiO_3$ ceramics[39] and that of $Nb_{Ti,Zr}$–V_{Pb} clusters was suggested in 12 at. % Nd doped PZT52/48 sputtered thin films.[3]

The capacitance–voltage (C–V) curves measured at 100 kHz are shown in Fig. 4(a). The butterfly like curves are shifted to the
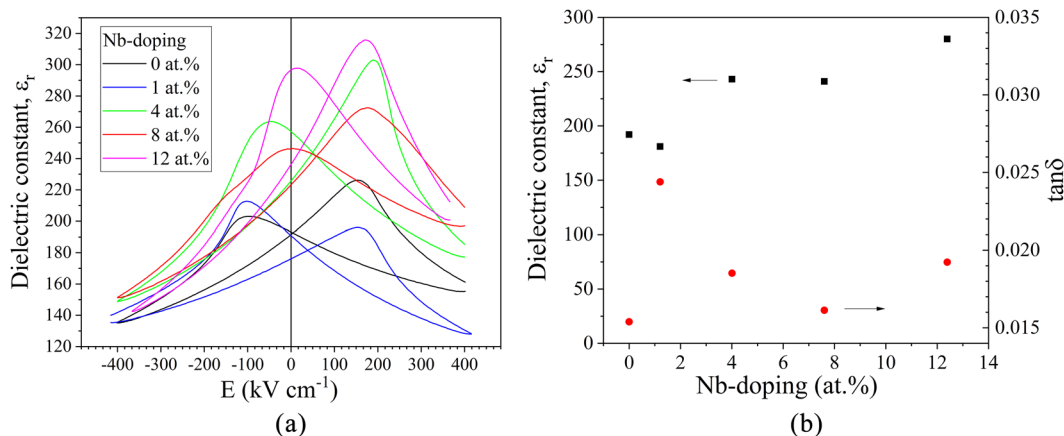

FIG. 4. (a) Dielectric constant as a function of the applied field. (b) Dielectric constant and tan δ at the crossover point as a function of Nb-doping. Measurements are at 100 kHz.

positive field direction due to the internal field, as will be discussed below. The dielectric constants, ε_r, and losses, $\tan \delta$, measured at the crossover point as a function of Nb-doping are shown in Table I and Fig. 4(b). There appeared to be a slight increase in the value of the dielectric constant with the extent of Nb-doping. The values are close to those measured previously on thin films with similar compositions: sputtered PZT25/75 ($\varepsilon_r = 300$)[29,40] and PZT24/76 ($\varepsilon_r = 246$ and $\tan \delta = 0.06$).[41] The low value of $\tan \delta$ could be attributed to the stabilization of domain wall movement by the internal field (as will be discussed below). The dielectric constants appeared to be lower than in bulk ceramics,[14] although it has been shown that the values of the dielectric constant close to the bulk were measured when the thickness of the films exceeded 3–4 μm in 62/38 PZT films.[42] The increase in the dielectric constant with the film thickness formed by sol–gel was attributed to the increased density with increasing thickness.[16] The contradictory behavior of Nb-doping on the values of the dielectric constant and $\tan \delta$ has been reported. Nb-doping has been reported to monotonically increase the dielectric constant in sputtered PZT52/48[27] and sol–gel PZT40/60,[21] PZT20/80,[12] and PZT40/60[23] films. The dielectric constant maximizes in PZT compositions close to MPB: at 1 at. % ($\varepsilon_r = 689$) of Nb in PZT53/47 films,[16] 2 at. % ($\varepsilon_r = 1100$) in sputtered PZT54/46 films,[28] 3 at. % ($\varepsilon_r = 2684$) in sol–gel PZT52/48 films,[43] 4 at. % ($\varepsilon_r = 1412.5$) in PZT52/48 films,[9] and 4 at. % (around $\varepsilon_r = 600$) in bulk PZT53/47 ceramics.[7] The increase in ε_r is explained by a decrease in the oxygen vacancy concentration with Nb-doping and thus a reduction in the number of domain pinning sites. The observed decrease in the dielectric constant in PZT53/47 films was explained by the increased content of the pyrochlore phase and/or reduction in grain size leading to relaxor type behavior.[5] However, the decrease in ε_r was often observed within the solid solution region where no pyrochlore phase was detected.[28] Alternately, the decrease in ε_r was explained by the formation of the PbO phase, which inhibited domain wall movement.[9] In several studies, dielectric properties degraded with Nb-doping: the values of ε_r decreased whereas $\tan \delta$ increased with Nb-doping in PZT53/47 sol–gel films[17] and both ε_r and $\tan \delta$ decreased with Nb-doping in sol–gel films with similar MPB composition PZT53/47.[20]

Leakage currents measured at 8 kV cm^{-1} were within the range 10^{-8}–10^{-7} A cm^{-2} for films with up to 8 at. % Nb (Table II) and did not show any clear dependence on Nb-doping up to this level. Typically, a decrease in the leakage current with Nb-doping was observed[28] related to the charge compensation of Nb^{5+} ions by the decrease in oxygen vacancies and thus a reduction in the number of free electrons caused by oxygen vacancies.[21] This would agree with

our observations up to 8 at. % Nb. There is a significant increase in leakage current at 12 at. % Nb, but this could be associated with an increase in second phases at such high doping levels. No clear dependence of the leakage current with the applied voltage was observed (Fig. S2 of the supplementary material).

The P–E loops of sputtered films are shown in Fig. 5. No dependence of the measurement frequency (1–100 Hz) on the shape of the P–E loop was observed, suggesting negligible contribution of the leakage and fast domain switching. The maximum polarization, P_{max}, and remanent polarization measured upon a decrease in field, P_r^+, and an increase in field, P_r^-, increased with Nb-doping up to 4 at. % (Table II). A further increase in doping resulted in the decrease in the polarization parameters. The polarization parameters were shown to exhibit maximum with Nb-doping: at 1 at. % Nb in sol–gel films grown at 600 °C ($P_r = 20$ μC cm^{-2});[16] at 2 at. % Nb in sol–gel PZT53/47 ($P_r = 25$ μC cm^{-2}) films,[18] in sol–gel PZT53/47 ($P_r = 30$ μC cm^{-2}) films,[25] in sol–gel PZT52/48 ($P_r = 14$ μC cm^{-2}) films,[9] and in sputtered PZT54/46 films ($P_r = 21$ μC cm^{-2});[28] at 3.5 at. % Nb in sol–gel PZT52/48 (43.4 μC cm^{-2}) films;[43] at 4 at. % Nb in bulk PZT53/47 ($P_r = 17$ μC cm^{-2}) ceramics;[7] and at 12 at. % Nb in sputtered PZT52/48 (40 μC cm^{-2}) films.[3] However, sol–gel grown PZT53/47 films showed a decrease in P_r with Nb-doping, from 31 μC cm^{-2} in undoped PZT to 17 μC cm^{-2} at 5 at. % Nd.[17] The degree of preferred orientation in crystallites affects the values of polarization. P_r was shown to decrease linearly with the decrease in the fraction of c-oriented grains. This is to be expected in a tetragonal composition as the displacement along the c-axis contributes directly to the film polarization.[44] Large values of P_r (70 μC cm^{-2}) and E_c (110 kV cm^{-1}) were measured for (100) oriented 2 at. % Nb-doped sol–gel PZT30/70 of composition similar to the one used in this work.[10] In order to minimize the effect of the degree of preferred orientation in the films on the polarization, the polarization values were normalized to 100% (111) orientation (inset of Fig. 5). The observed trend of the polarization exhibiting maximum values at 4 at. % Nd-doping is clearly demonstrated. Alternatively, the observed decrease in P_r and P_{max} in PZT53/47 sol–gel films with Nb-doping was related to the decrease in BO$_6$ octahedral volume upon substitution of smaller Nb on the B-site.[5] Finally, the decrease in P_r was associated with the presence of the pyrochlore phase.[18]

In this work, due to the asymmetry P–E loops, the average value of the coercive field is assessed as $(E^+ + E^-)/2$. This exhibited a maximum value at 4 at. % Nb (Fig. 6). The increase is likely to be caused by the increased fraction of (100) orientation and/or the number of B-site vacancies, which may be effective pinning sites.

TABLE II. Effect of Nb-doping on the leakage current density, parameters of P–E loops, and photocurrent.

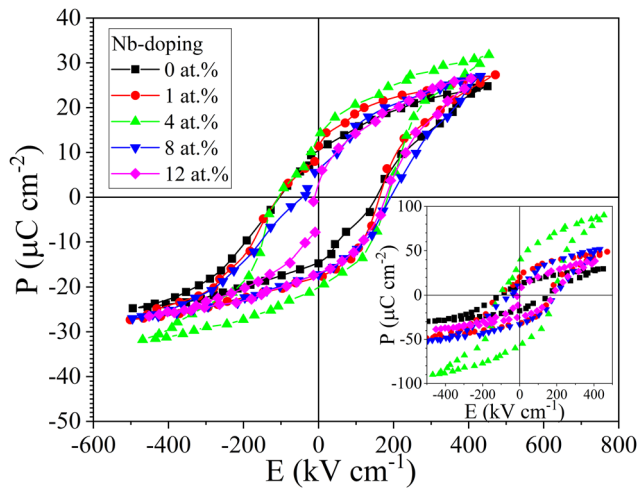| Nb-doping (at. %)	Leakage current density (A cm^{-2})	P_{max} (μC cm^{-2})	P_r^+ (μC cm^{-2})	P_r^- (μC cm^{-2})	E_C^+ (kV cm^{-1})	E_C^- (kV cm^{-1})	E_i (kV cm^{-1})
0	1.9×10^{-7}	24.8	10.4	−14.7	154.8	−103.8	−25.5
1	2.5×10^{-7}	27.3	11.4	−17.8	162.4	−106.8	−27.8
4	2.3×10^{-7}	37.8	13.5	−20.1	184.6	−106.4	−39.1
8	1.1×10^{-8}	27.0	6.2	−17.2	191.9	−40.8	−75.6
12	9.6×10^{-7}	26.5	3.2	−16.9	179.2	−10.6	−84.3

FIG. 5. P–E loops of Nb-doped PZT films. Measurement at 1 Hz. The inset shows polarization values normalized by the degree of (111) preferential orientation of PZT.

Previous reports showed maximum values of the coercive field at 2 at. % Nb in sol–gel PZT53/47 (100 kV cm^{-1}) films,[18] 3 at. % Nb in sol–gel PZT53/47 (43 kV cm^{-1}) films,[16] and 5 at. % in sol–gel grown PZT53/47 (52 kV cm^{-1}) films[17] and decreased upon further doping. However, in most studies, the coercive field decreased with Nb-doping in PZT films [7,9,19,23,43] or was independent of doping as in sputtered PZT54/46 films (E_C = 38 kV cm^{-1}).[28] The decrease in the coercive field was attributed to the increased mobility of domain walls resulting from the decreased concentration of oxygen vacancies. In the vicinity of the MPB composition, Nb-doping promoted the formation of the rhombohedral phase with eight equivalent polarization orientations as opposed to 2 in tetragonal phase, thus reducing E_c.[22] In 2 at. % Nb-doped PZT60/40 films, higher values of P_r and E_c were measured in (001) oriented films as compared to the
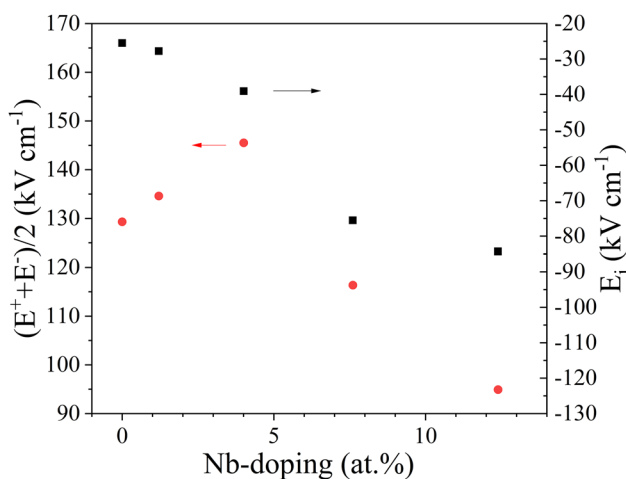

FIG. 6. $(E^+ + E^-)/2$ and E_i as a function of Nb-doping.

(111) oriented films: 71.9 μC cm^{-2}, 63.7 kV cm^{-1} and 65.3 μC cm^{-2}, 41.3 kV cm^{-1}, respectively.[6]

The P–E hysteresis curves show a shift in the positive direction due to the presence of the internal field. The internal field, E_i, was calculated as follows[45] and is shown in Fig. 6:

$$E_i = -\frac{E_c^+ + E_c^-}{2}.$$

The negative values of E_i (when the DRIVE port of the Radiant tester is connected to the top electrode) observed in this work implied that the direction of the internal field was oriented toward the top electrode. The negative values of E_i increased with the Nb-doping range studied in this work (up to 12 at. %). The magnitude of the internal field observed in this work is close to the values reported for PLD grown films where E_i decreased with the increase in Zr content (E_i = −47.8 kV cm^{-1} for PZT20/80 and E_i = −16.7 kV cm^{-1} for PZT40/60[26]) and for sputtered[41] PZT films. Negative E_i of 70 kV cm^{-1} was observed in (111) PZT25/75 films,[46] whereas positive values of E_i were reported for sol–gel PZT53/47 films. [16,17] Nb-doping resulted in an increase in the negative values of E_i in sputtered PZT52/48 films.[4,27] The internal field increased monotonically from −1 kV cm^{-1} for undoped sputtered PZT54/46 to −3.5 kV cm^{-1} for 7 at. % Nb-doped PZT54/46 films.[28] No internal field was observed in undoped sol–gel PZT20/80 films, whereas negative E_i was observed upon 4 at. % Nb-doping.[19] The internal field in Nb-doped PZT changed sign from positive to negative when the thickness of the film increased in sol–gel PZT30/70 films.[10]

Several mechanisms have been proposed to explain the origin of the internal field. It has been suggested that the induced stresses in the film align the polarization axis to a particular direction.[27] Alignment of the dipoles consisting of positively (e.g., oxygen vacancy or Nb$_{Ti}$) and negatively (cation vacancies) charged defects in the bulk was reported as the origin of the internal field.[16,26,28,47] Finally, the origin of the internal field was attributed to the asymmetry of the Schottky contacts between the film and the top and bottom electrodes. The internal field increased when a Ba(Mg$_{1/3}$Nb$_{2/3}$)O$_3$ buffer layer was deposited on a Pt electrode in sol–gel PZT52/48 films.[43] The internal field observed in PZT45/55 thin films grown by sol–gel and sputtering was related to the Schottky barrier at the bottom Pt–PZT interface.[48] The presence of negative Pb vacancies close to the top electrode was suggested as the origin of the polarity dependence in the dielectric constant in PZT40/60 sol–gel films.[21] In this study, the film growth conditions (including the film thickness) and electrode fabrication techniques were similar for all films and were unlikely to cause systematic changes in the stresses and/or asymmetry of the Schottky barriers. As a result, we believe that the monotonic increase in negative values of E_i with Nb-doping is likely to be caused by the alignment of the increased number of oppositely charged defects (e.g., Nb$_{Ti}$ and $V_{Ti,Zr}''''$).

The time dependence of the temperature gradient, $\frac{\partial T}{\partial t}$, and pyroelectric current, I, are shown for a 4 at. % Nb-doped sample biased by −30 V [Fig. 7(a)]. The negative minimum of the current is slightly shifted from the maximum value of the temperature gradient. The shift is thought to be caused by a small time lag in heat propagation between the Pt-resistive thermometer and the thin film. It was assumed that the negative minimum value of the measured
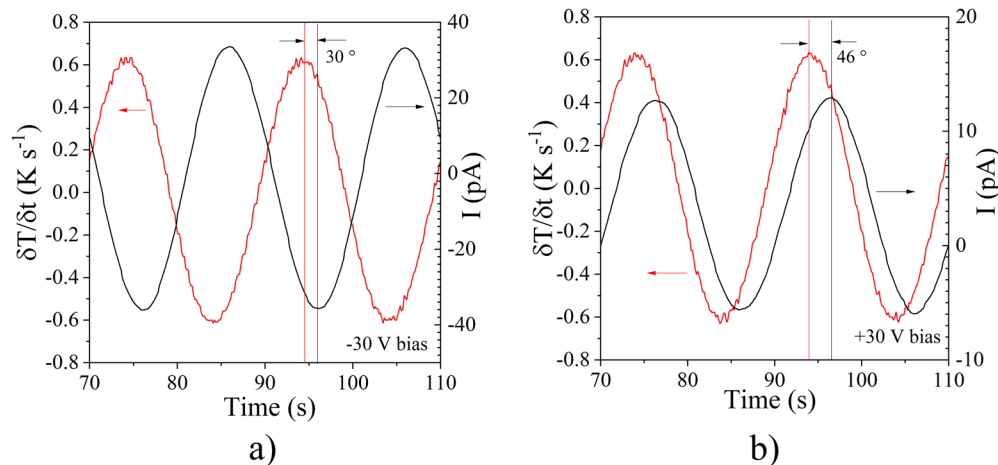
FIG. 7. Pyroelectric measurements of 4 at. % Nb-doped PZT films poled at −30 V (a) and poled at +30 V (b). Phase shift (in degree) between the maximum of $\frac{\partial T}{\partial t}$ and the maximum/minimum of the pyroelectric current is given.

current corresponded to the maximum value of the temperature gradient, resulting in negative values of the pyroelectric coefficient. On few occasions, the maximum values of the temperature gradient corresponded to the positive maximum of the current, resulting in positive values of the pyroelectric coefficient, as shown in Fig. 7(b) for a +30 V biased 4 at. % doped film. The pyroelectric coefficient, p, is calculated as follows:

$$ p = \frac{I}{A \times \frac{\partial T}{\partial t}}, $$

where I is the pyroelectric current and A is the surface area of the top electrode. The values of the pyroelectric coefficient were independent of the top electrode surface area (0.5, 1, 2, and 3 mm in diameter). However, in this study, results for 0.5 mm electrodes are present as larger electrodes occasionally exhibited short-circuit behavior presumably due to the presence of the defects in the grown films. The pyroelectric coefficients of unpoled films are shown in Fig. 8. The pyroelectric coefficient of the undoped film measured in the work (-7.7×10^{-5} C m^{-2} K^{-1}) is lower than the reported values of -2×10^{-4} C m^{-2} K^{-1} of self-poled sputtered PZT25/75 films with close composition.[29,40] The pyroelectric coefficient of the unpoled film increased with Nb-doping and reached constant values at 8 at. % Nb-doping. This increase could be related to the increase in E$_i$ caused by Nb-doping [Fig. 8(b)] and thus increased self-poling of the films. The pyroelectric coefficient exhibited maximum with Nb-doping at 1 at. % Nb (-4.6×10^{-4} C m^{-2} K^{-1}) in sol–gel films,[12] at 2 at. % Nb (-3.5×10^{-4} C m^{-2} K^{-1}) in PZT53/47 films,[25] and at 4 at. % Nb (-1.02×10^{-4} C m^{-2} K^{-1}) in doped PZT53/47 bulk ceramics.[7]

The effect of poling on the pyroelectric coefficient was studied by applying consequently 10, 20, and 30 V to the top electrode as positive and negative bias for 3 min followed by the pyroelectric evaluation (Fig. 9). Dielectric properties, leakage currents (at 8 kV cm^{-1}), and P–E loops were re-measured after the pyroelectric evaluation of poled samples. A slight decrease in ε_r and increase in tan δ were observed after poling (Fig. S3 of the

supplementary material). No changes in the P–E loop shape were observed after poling, and only a slight increase in the leakage current was detected. The pyroelectric coefficient increased with the negative bias and reached a plateau. During the positive poling, the pyroelectric coefficient decreased and in several cases became positive. The observed behavior could be related to the presence of the internal field in the films. The large negative values of the internal field present in the as-deposited films enhanced the pyroelectric response due to self-poling, which showed only a small increase (less than 20%) during negative biasing. Previously, it was shown that self-poled sputtered (111) PZT25/75 films could not be poled further by application of 250 kV cm^{-1} field.[46] The values of the pyroelectric coefficient approaching zero were attained when the applied positive bias was close to the compensation of the negative internal potential.
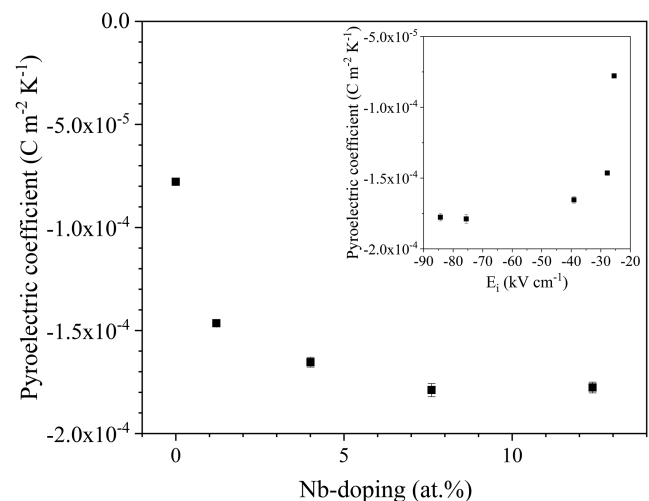

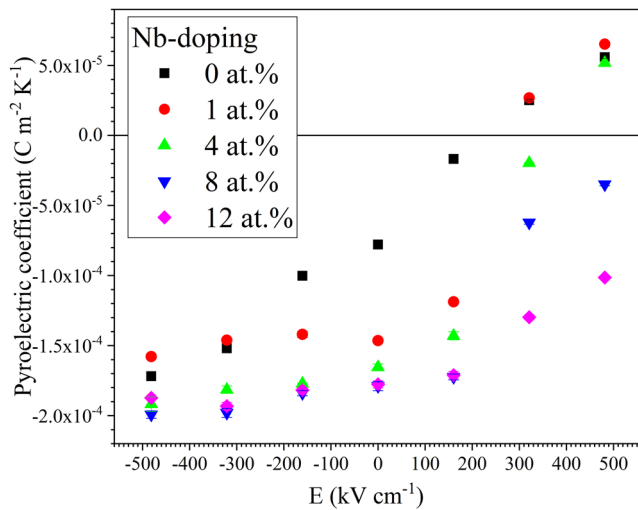**FIG. 8.** Pyroelectric coefficient of unpoled samples as a function of doping (a) and internal field, E$_i$ (inset).

FIG. 9. Pyroelectric coefficients of Nb-doped PZT films as a function of the applied field.

FIG. 10. P–E loops of the 4 at. % Nb doped sample with and without light irradiation.

This position shifted to more positive values of bias with doping, concurrent with the increasing negative values of the internal field. Further positive biasing caused the reversal of the polarity of the electrode polarization, which led to the change of sign [Fig. 7(b)] and the increase in the pyroelectric coefficient. Pyroelectric coefficients did not appear to increase linearly with the remnant polarization in contrast to the observed linear increase in sputtered (111) PZT15/85 films.[49] During heating, positive current was observed to flow from the bottom electrode and the direction of polarization was attributed from the bottom to the top electrode.[41] A similar effect of the applied bias on the values of the piezoelectric coefficient, d_{31}, was observed in $Pb_{1.1}Nb_{0.04}Zr_{0.2}Ti_{0.8}O_3$ sol–gel films with the relatively close Zr/(Zr + Ti) ratio.[19] However, the polarity of the top electrode appeared to be opposite to the one found in this study.

Several electrodes showed the formation of small circular defects concentrated close to the edge of the top electrode after poling at ±30 V (Fig. S4 of the supplementary material). The leakage current and P–E loops collected after the bias did not show deterioration of properties due to the electrical breakdown process. It is possible that the defects resulted from a self-healing breakdown, where the heat generated by the localized breakdown resulted in local evaporation of the electrode material, thus preventing short-circuiting through the damaged region.[50]

Recently, the photovoltaic response in perovskite ceramics has attracted renewed interest.[51] The effect originates from the production of an electron–hole pair upon irradiation with phonon energy higher than the bandgap of the material followed by their separation under an electric field. The nature of this electric field is still not fully resolved. It can be developed in the bulk of a ferroelectric material, at domain walls, or caused by the difference in Schottky barrier heights at metal/ceramic interfaces or the depolarization field.[51,52] No changes in the P–E loop shape were observed when measured under illumination (Fig. 10). The measured light intensity as a function of wavelength is given in the supplementary
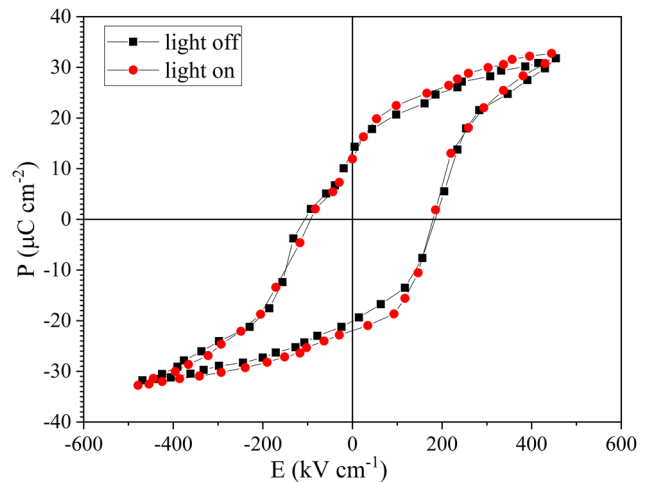
material (Fig. S5). A reduction in the saturation polarization and a shift of the loop along the y axis was reported previously in sol–gel deposited $(Pb_{0.93}La_{0.07})(Zr_{0.6}Ti_{0.4})O_3$ thin films when irradiated with 3.4 eV Hg lamp light at a slightly lower frequency of P–E loops of 0.1 Hz as compared to the one used in this work (−1 Hz).[53] The ferroelectric (FE) loop was reported to become leakier, with increased values of both polarization and coercive field upon illumination of $Pb[(Mg_{1/3}Nb_{2/3})_{0.68}Ti_{0.32}]O_3$ crystals.[54]

Photocurrent ($I_{photo} = I_{light} − I_{dark}$) was detected in all the films studied. Before the effect of light irradiation on various properties of PZT films are discussed, we need to consider light pathways to the PZT material located between the electrodes. We expect significant light absorption and reflection in the top electrode formed of 40 nm of Au and 10 nm of Ti layers. For example, for thinner 33 nm Au films, the maximum transmission was only 15% at 500 nm and significantly decreased with the wavelength, especially in the vicinity of the PZT bandgap region (309 nm as discussed below).[55] In addition to the light penetrating through the top electrode, some waveguiding effects to the PZT material positioned between the electrodes from the electrode edge are expected as an extended light source was employed at about 10 cm from the film surface. However, the irradiated area is expected to be small due to the extensive light absorption in PZT. In both cases, the amount of light reaching the PZT layer is thought to be small. As a result, the photovoltaic response described in this work is expected to increase when transparent electrodes are employed (e.g., ITO). In order to evaluate the effect of the Au thickness on the photovoltaic properties, we deposited Au(13 nm)/Ti(10 nm) electrodes (0.5 mm in diameter). An increase in the photocurrent (up to 69% for the 8 at. % Nb-doped sample) was observed except for the 4 at. % Nb-doped sample. However, due to mechanical damage by the measuring probes, no further evaluation using thin Au(13 nm)/Ti(10 nm) electrodes was performed. No correlation was observed between the magnitude of photocurrent with Nb-doping and the internal field, E_i. However, the magnitude of the photocurrent appeared to increase with the A/B ratio (inset of Fig. 11). The magnitude of the photocurrent is proportional to the rate of photocarrier generation and thus the width of the bandgap in
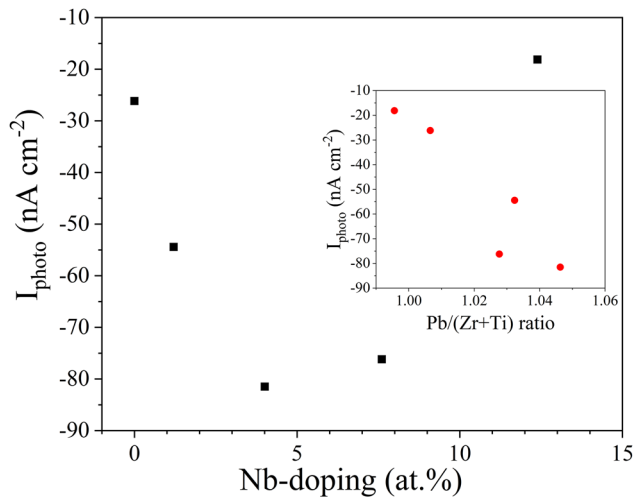
FIG. 11. I_{photo} as a function of Nb-doping of unpoled samples. The inset shows I_{photo} as a function of Pb/(Zr + Ti) ratio. 13 nm Au thick top electrodes were employed.

FIG. 12. I_{photo} as a function of temperature. The inset shows the temperature gradient of I_{photo} as a function of I_{photo} at 25 °C. 13 nm Au thick top electrodes were employed.

PZT. The bandgap showed a weak dependence on the Zr/Ti ratio in sol–gel PZT films[56] and was calculated from optical measurement to be about 4 eV (309 nm) for PZT30/70.[26] Occasionally, the photocurrent was observed when epitaxial PZT films were irradiated using light with sub-band photon energy[26] and was assigned to the release of trapped carries from deep trapping levels. The defects can reduce the bandgap by introducing acceptor or donor states. For example, the doping of Ni^{2+} on the B-site of $[KNbO_3]_{1-x}[BaNi_{1/2}Nb_{1/2}O_{3-\delta}]_x$ introduced hybridized Ni 3d and O 2p states in the valence band and reduced bandgap[57] and the oxygen vacancies in $BaTiO_3$ introduced donor states in the bandgap, reducing it from 3.3 to 2.75 eV.[58] Contradictory reports on the effect of Nb-doping on the bandgap in PZT have been published. The bandgap decreased during 2 at. % Nb-doping in sol–gel PZT52/48,[59] increased during 4 at. % Nb-doping in sol–gel PZT65/35,[60] or was not significantly affected by a small degree of Nb-doping in sol–gel PZT20/80 (4 at. %).[56] The weak dependence of the bandgap on the extent of Nb-doping is consistent with the observation that photocurrent did not show a linear dependence with Nb-doping in our films. We can speculate that the observed increase in photocurrent with the A/B ratio was related to the increased number of B-site vacancies when the A/B ratio was greater than 1. The dielectric constant and $\tan \delta$ increased slightly upon irradiation, especially at lower frequencies, presumably due to the photocurrent contribution to the losses (Fig. S3 of the supplementary material).

Within the narrow temperature range close to RT (16–32 °C), the temperature dependences of the photocurrent can be assumed to be linear (Fig. 12). The negative values of the temperature gradient of the photocurrent monotonically decreased with the magnitude of the photocurrent (inset of Fig. 12). The temperature dependence of the photocurrent affected the results of pyroelectric measurements when measured under continuous light illumination (Fig. 13). The temperature of the sample stage due to the light illumination increased by only 0.4 K as the lamp was fitted with an IR filter and no effect on the magnitude of temperature oscillations was observed.
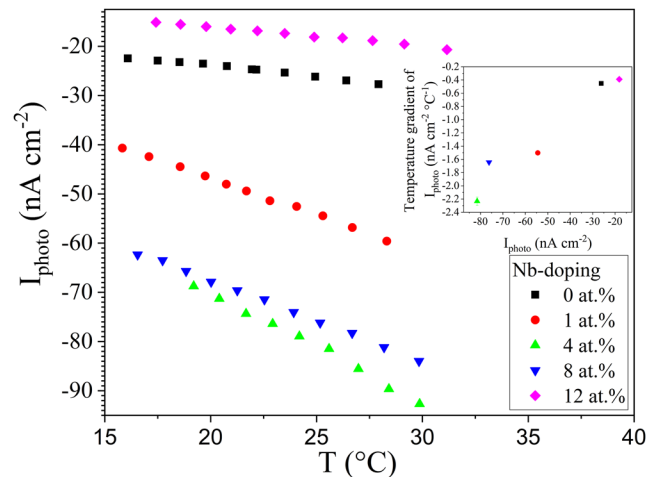
However, in several experiments, the magnitude of the pyroelectric current oscillations was increased and the values were shifted toward more negative values. The magnitude of the shift was close to the value of the photocurrent. The combined current oscillations calculated by the addition of thermally induced changes in the photocurrent and the pyroelectric current (52.3 pA for 4 at. % Nd doped film) agreed reasonably well with the experimentally measured current oscillations upon illumination (54.1 pA). Furthermore, the increase in the phase shift between the minimum of the current and the maximum of the temperature gradient was assigned to the increased contribution of the 90° phase difference between the changes in pyroelectric current and photocurrent. In several cases, the phase difference of the pyroelectric current and the photocurrent resulted in the decrease in the current oscillations. The largest contribution
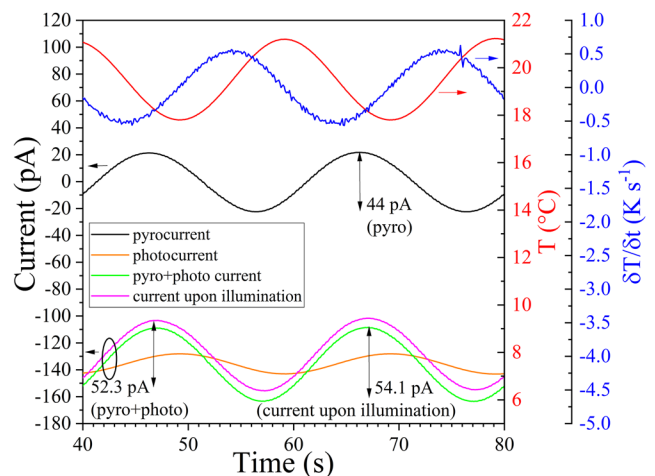

FIG. 13. Current as a function of time for an unpoled 4 at. % Nb-doped sample during pyroelectric measurements with and without illumination. A 13 nm Au thick top electrode was employed.

of the photocurrent was observed in 4 at. % Nb-doped films poled at −30 V, resulting in a 47% increase in the magnitude of the current oscillations upon light illumination. The combined pyroelectric and photovoltaic effect may be used to enhance the sensitivity of pyroelectric devices when appropriate background illumination is used. For example, the combination of photovoltaic and pyroelectric effects in $BaTiO_3$ was exploited as a self-powered photodetector[58] where the increase in the sample temperature upon pulsed light irradiation resulted in increased combined photovoltaic and pyroelectric current.

CONCLUSIONS

PZT30/70 thin films with up to 12 at. % Nb were grown by co-sputtering from ceramic PZT and metallic Nb targets at 600 °C. Within the solid solution region (up to 4 at. %), Nb-doping decreased the preferred (111) orientation, increased c/a tetragonality, and enhanced remanent polarization. The measured A/B perovskite ratio was greater than 1 and was assigned to the formation of B-site vacancies. Internal fields produced asymmetric FE loops and increased with the extent of Nb-doping. Pyroelectric coefficients increased with Nb-doping and showed a complex dependence on the applied bias due to the presence of the internal field. Photocurrent was detected in all films and increased with the A/B ratio. The combined photovoltaic–pyroelectric effect increased the values of the measured current by up to 47% upon light illumination.

SUPPLEMENTARY MATERIAL

See the supplementary material for additional characterization of dielectric and photovoltaic properties.

ACKNOWLEDGMENTS

DATA AVAILABILITY

The data that support the findings of this study are available from the corresponding author upon reasonable request.

REFERENCES

[1] P. K. Panda and B. Sahoo, Ferroelectrics **474**, 128 (2015).

[2] R.-A. Eichel, J. Electroceram. **19**, 11 (2007).

[3] C. S. Han, K. S. Park, H. J. Choi, and Y. S. Cho, ACS Appl. Mater. Interfaces **9**, 18904 (2017).

[4] J.-S. Yang, Y. Kang, I. Kang, S. Lim, S.-J. Shin, J. Lee, and K. H. Hur, IEEE Trans. Ultrason., Ferroelectr., Freq. Control **64**, 617 (2017).

[5] S. B. Majumder, B. Roy, R. S. Katiyar, and S. B. Krupanidhi, J. Appl. Phys. **90**, 2975 (2001).

[6] W. Gong, J.-F. Li, X. Chu, Z. Gui, and L. Li, Appl. Phys. Lett. **85**, 3818 (2004).

[7] A. Tripathi, A. K. Tripathi, T. C. Goel, and P. K. C. Pillaiet, in *9th International Symposium on Electrets (ISE 9) Proceedings* (IEEE, 1996), p. 878.

[8] D. Dimos, R. W. Schwartz, and S. J. Lockwood, J. Am. Ceram. Soc. **77**, 3000 (1994).

[9] Q. Li, X. Wang, F. Wang, J. Dou, W. Xu, and H. Zou, J. Ceram. Sci. Technol. **8**, 519 (2017).

[10] Z.-X. Zhu, C. Ruangchalermwong, and J.-F. Li, J. Appl. Phys. **104**, 054107 (2008).

[11] T. Fujii, T. Naono, A. Mukaiyama, T. Arakawa, Y. Hishinuma, Y. Li, and J. Birkmeyer, Fujifilm Research and Development No. 59–2014, 2014, p. 32.

[12] H. Han, S. Kotru, J. Zhong, and R. K. Pandey, Infrared Phys. Technol. **51**, 216 (2008).

[13] Y. Xu, A. Ignatiev, N. Wu, and Y. Wang, in *AeroSense'99* (SPIE, 1999), p. 338.

[14] M. Pereira, A. G. Peixoto, and M. J. M. Gomes, J. Eur. Ceram. Soc. **21**, 1353 (2001).

[15] Z. Ujma, L. Szymczak, J. Hańderek, K. Szot, and H. J. Penkalla, J. Eur. Ceram. Soc. **20**, 1003 (2000).

[16] V. Kayasu and M. Ozenbas, J. Eur. Ceram. Soc. **29**, 1157 (2009).

[17] R. Kurchania and S. J. Milne, J. Sol-Gel Sci. Technol. **28**, 143 (2003).

[18] R. D. Klissurska, K. G. Brooks, I. M. Reaney, C. Pawlaczyk, M. Kosec, and N. Setter, J. Am. Ceram. Soc. **78**, 1513 (1995).

[19] C. Nistorica, J. Zhang, P. Padmini, S. Kotru, and R. K. Pandey, Integr. Ferroelectr. **63**, 49 (2004).

[20] K. W. Kwok, K. P. Kwok, R. C. W. Tsang, H. L. W. Chan, and C. L. Choy, Integr. Ferroelectr. **80**, 155 (2006).

[21] W. Sik Kim, S.-M. Ha, H.-H. Park, and C. Eun Kim, Thin Solid Films **355-356**, 531 (1999).

[22] D. F. Ryder and N. K. Raman, J. Electron. Mater. **21**, 971 (1992).

[23] E. C. F. Souza, A. Z. Simões, M. Cilense, E. Longo, and J. A. Varela, Mater. Chem. Phys. **88**, 155 (2004).

[24] C. K. Barlingay and S. K. Dey, Thin Solid Films **272**, 112 (1996).

[25] K. W. Kwok, R. C. W. Tsang, H. L. W. Chan, and C. L. Choy, J. Appl. Phys. **95**, 1372 (2004).

[26] L. Pintilie, I. Vrejoiu, G. Le Rhun, and M. Alexe, J. Appl. Phys. **101**, 064109 (2007).

[27] T. Fujii, Y. Hishinuma, T. Mita, and T. Arakawa, Solid State Commun. **149**, 1799 (2009).

[28] T. Haccart, D. Remiens, and E. Cattan, Thin Solid Films **423**, 235 (2003).

[29] R. Köhler, G. Suchaneck, P. Padmini, T. Sandner, G. Gerlach, and G. Hofmann, Ferroelectrics **225**, 57 (1999).

[30] T. Maeder and P. Muralt, MRS Online Proc. Libr. **341**, 361 (1994).

[31] I. Lubomirsky and O. Stafsudd, Rev. Sci. Instrum. **83**, 051101 (2012).

[32] P. Zaumseil, J. Appl. Crystallogr. **48**, 528 (2015).

[33] Z. Huang, Q. Zhang, and R. W. Whatmore, J. Mater. Sci. Lett. **17**, 1157 (1998).

[34] Z. Huang, Q. Zhang, and R. W. Whatmore, J. Appl. Phys. **86**, 1662 (1999).

[35] P. Muralt, S. Hiboux, C. Mueller, T. Maeder, L. Sagalowicz, T. Egami, and N. Setter, Integr. Ferroelectr. **36**, 53 (2001).

[36] R. W. Whatmore, Z. Huang, and M. Todd, J. Appl. Phys. **82**, 5686 (1997).

[37] R. D. Shannon, Acta Crystallogr., Sect. A **32**, 751 (1976).

[38] D. J. Keeble, S. Singh, R. A. Mackie, M. Morozov, S. McGuire, and D. Damjanovic, Phys. Rev. B **76**, 144109 (2007).

[39] R. A. Mackie, A. Peláiz-Barranco, and D. J. Keeble, Phys. Rev. B **82**, 024113 (2010).

[40] P. Padmini, R. Köhler, G. Gerlach, R. Bruchhaus, and G. Hofmann, J. Phys. IV **08**, Pr9–151 (1998).

[41] R. Bruchhaus, D. Pitzer, M. Schreiter, and W. Wersing, J. Electroceram. **3**, 151 (1999).

[42] K. Sreenivas and M. Sayer, J. Appl. Phys. **64**, 1484 (1988).

[43] Y. Shao, J. Zhou, W. Chen, J. Shen, and Z. Wang, J. Mater. Sci.: Mater. Electron. **31**, 9928 (2020).

[44] H. Morioka, G. Asano, T. Oikawa, H. Funakubo, and K. Saito, Appl. Phys. Lett. **82**, 4761 (2003).

[45] S. Sun, Y. Wang, P. A. Fuierer, and B. A. Tuttle, Integr. Ferroelectr. **23**, 25 (1999).

[46]R. Köhler, N. Neumann, N. Heß, R. Bruchhaus, W. Wersing, and M. Simon, Ferroelectrics **201**, 83 (1997).

[47]S. Okamura, S. Miyata, Y. Mizutani, T. Nishida, and T. Shiosaki, Jpn. J. Appl. Phys., Part 1 **38**, 5364 (1999).

[48]A. L. Kholkin, K. G. Brooks, D. V. Taylor, S. Hiboux, and N. Setter, Integr. Ferroelectr. **22**, 525 (1998).

[49]M. Kohli and P. Muralt, Ferroelectrics **225**, 155 (1999).

[50]J. E. Carnes and M. T. Duffy, J. Appl. Phys. **42**, 4350 (1971).

[51]C. Paillard, X. Bai, I. C. Infante, M. Guennou, G. Geneste, M. Alexe, J. Kreisel, and B. Dkhil, Adv. Mater. **28**, 5153 (2016).

[52]Y. Yuan, Z. Xiao, B. Yang, and J. Huang, J. Mater. Chem. A **2**, 6027 (2014).

[53]D. Dimos, W. L. Warren, M. B. Sinclair, B. A. Tuttle, and R. W. Schwartz, J. Appl. Phys. **76**, 4305 (1994).

[54]A. S. Makhort, F. Chevrier, D. Kundys, B. Doudin, and B. Kundys, Phys. Rev. Mater. **2**, 012401 (2018).

[55]A. Axelevitch, B. Gorenstein, and G. Golan, Phys. Procedia **32**, 1 (2012).

[56]H. Lee, Y. S. Kang, S.-J. Cho, B. Xiao, H. Morkoç, T. D. Kang, G. S. Lee, J. Li, S.-H. Wei, P. G. Snyder, and J. T. Evans, J. Appl. Phys. **98**, 094108 (2005).

[57]I. Grinberg, D. V. West, M. Torres, G. Gou, D. M. Stein, L. Wu, G. Chen, E. M. Gallo, A. R. Akbashev, P. K. Davies, J. E. Spanier, and A. M. Rappe, Nature **503**, 509 (2013).

[58]N. Ma, K. Zhang, and Y. Yang, Adv. Mater. **29**, 1703694 (2017).

[59]S. Samanta, M. Rath, V. Sankaranarayanan, K. Sethupathi, and M. S. R. Rao, Phys. Status Solidi B **257**, 1900272 (2020).

[60]I. Boerasu, M. Pereira, M. J. M. Gomes, and M. I. C. Ferreira, J. Optoelectron. Adv. Mater. **2**, 602 (2000).